REMOTE SENS. ENVIRON. 48:347–357 (1994)

The Effects of Sensor Field-of-View on the Geometrical Characteristics of Sea Ice Leads and Implications for Large-Area Heat Flux Estimates

J. Key, J. A. Maslanik,* and E. Ellefsen**

The release of heat from sea ice fractures ("leads") is an important component of the heat budget in the Arctic, but their impact on regional scale climate is difficult to assess without more information on their distribution in both space and time. Remote sensing of leads using satellite data, specifically AVHRR thermal and Landsat visible-band imagery, is examined empirically with respect to lead width, orientation, and area fraction. The geometrical aspects of the sensor are simulated so that the effect of sensor field-of-view on retrieved lead width statistics can be assessed. This is done using Landsat data and simulated lead networks degraded to AVHRR pixel sizes. The analyses illustrate how leads of sufficiently high contrast tend to "grow" with increasing pixel size and how small or low contrast leads disappear. The relationship between lead contrast and the width/field-of-view ratio is also examined in order to determine the limits of lead detectability, and illustrates the multivalued nature of the problem of lead width retrieval. To help quantify the importance of changes in lead statistics, turbulent heat flux is calculated as a function of lead width and lead fraction. It is shown that pixel size has a substantial effect on estimates of turbulent heat transfer from leads to the atmosphere.

INTRODUCTION

Fractures in the sea ice pack ("leads"), either open or refrozen, are an important component of local scale heat exchange in the Arctic, providing a significant source of heat and moisture to the atmosphere that is as much as 2 orders of magnitude greater than turbulent energy exchange from thick sea ice (Maykut, 1978). Lead coverage also affects the ice-pack albedo and, in turn, the rate of ice melt through the absorption of heat within the open-water leads (Maykut and Perovich, 1987). Modeling studies of the influence of sea ice leads on climate point out the importance of accurately representing lead fraction, which typically defines the proportion of open water within the interior pack ice (Ledley, 1988; Simmonds and Budd, 1990). Relatively large changes in lead coverage can be related to strong storms in the Arctic (Maslanik and Barry, 1989) and can contribute as a positive feedback to maintaining the strength of these storms (Ledrew et al., 1992). In addition to total lead-covered area, the widths of individual leads affects the rate of heat transfer from the ocean to the atmosphere (e.g., Andreas and Murphy, 1986). Unfortunately, relatively little information is available on the numbers, dimensions, and life cycle of leads in the Arctic ice pack. Remote sensing—in particular, the use of medium-resolution imagery from polar orbiters such as the NOAA Advanced Very High Resolution Radiometer (AVHRR)—offers the potential to develop a climatology of lead statistics that is well suited for climate studies and comparison to other remotely sensed data such as microwave imagery. However, before a consistent and accurate record of lead statistics can be obtained, it is necessary to understand how sensor characteristics, atmospheric properties, and surface conditions influence the detection and interpretation of sea ice leads in AVHRR and other satellite data.

The objectives of this work are to begin to define the sources and magnitudes of errors in retrieved lead statistics as a function of the spatial resolutions of existing and future sensors, and to assess the importance of these errors in a physical context. Specifically, we seek to determine the extent to which sensor field-of-view affects observations of lead geometries, and how this translates into changes in the exchange of sensible and latent heat from the ocean to the atmosphere. For

*Cooperative Institute for Research in Environmental Sciences, Division of Cryospheric and Polar Processes, University of Colorado, Boulder

Address correspondence to Jeffrey R. Key, CIRES, Univ. of Colorado, Campus Box 449, Boulder, CO 80309-0449.

Received 30 September 1992; revised 8 January 1994.

0034-4257/94/$7.00

655 Avenue of the Americas, New York, NY 10010

example, since the temperature contrast between open water and ice provides a means to map leads using thermal imagery, to what degree does this contrast affect the apparent width of a lead and our ability to detect leads and to accurately map their widths and areal coverage? Since the exchange of energy between the ocean and atmosphere is affected by all openings in the ice pack and not just those visible at certain scales, we need to know how well observations taken at different scales represent actual conditions. To address these questions, we compare lead statistics retrieved from satellite imagery of varying spatial resolution, and we examine whether lead statistics derived from "medium" resolution imagery (e.g., a field-of-view of 500–1000 m) can be used to estimate characteristics of lead distributions that would be obtained from higher-resolution images with a field-of-view of about 80 m. While the emphasis is on lead width—defined as the distance across a lead along a line perpendicular to the local orientation of the lead—, lead orientation, and fractional coverage are also examined. The effects of atmospheric effects on the retrieval of lead geometries is examined elsewhere (Stone and Key, 1993).

Other studies of the effect of sensor field-of-view (FOV) on parameter retrieval have appeared in the literature, including several that have addressed the effects on cloud amount and landcover mapping. Shenk and Salomonson (1972) and Wielicki and Welch (1986) studied cloud fraction where real and synthetic data containing cloud fields were degraded in resolution, and the fractional coverage was observed as a function of scale. In their investigation of the effect of FOV on landcover classification, Townshend and Justice (1988) and Woodcock and Strahler (1987) examined the image data variance as a function of measurement scale to determine the optimal resolution for monitoring purposes. Unfortunately, the results of those studies are difficult to generalize to other mapping requirements and image types. Here we present initial results toward quantifying these relationships for leads.

METHODS AND DATA

One way to investigate the effects of sensor field-of-view on retrieved lead statistics is to examine data from existing sensors of various spatial resolutions. For example, Figure 1 shows colocated data from the Landsat Multi-Spectral Scanner (MSS) (visible band), AVHRR (thermal band), and aircraft passive microwave imagery from the U.S. Navy K-band Radiometric Mapping System (KRMS) (33.6 Ghz, vertical polarization), for a portion of the Beaufort Sea in the western Arctic Ocean. Leads appear as the darker linear features within the surrounding ice pack, and are differentiated based on their lower albedo and higher physical and microwave

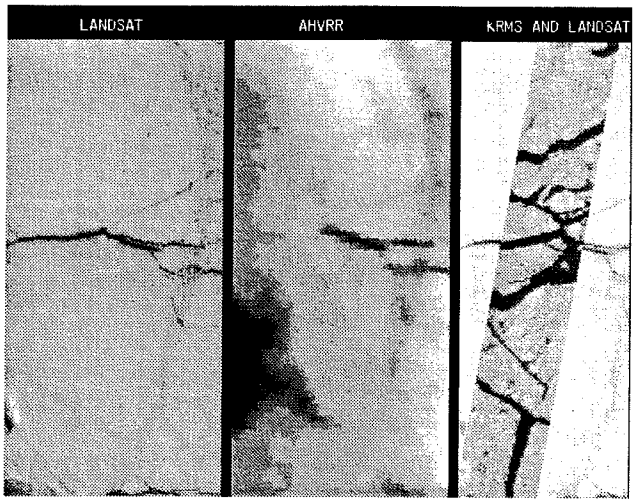

Figure 1. Colocated Landsat, AVHRR, and KRMS imagery of sea ice leads in the Beaufort Sea.

brightness temperatures than the thicker sea ice. While the same general lead structure is apparent in the images, the smaller leads are obviously harder to detect in the AVHRR image (nadir FOV of 1.1 km) than both the Landsat image (80 m FOV) and the KRMS data (26 m FOV at flight altitude of 1500 m). In addition to the differences in spatial resolution, each sensor is sampling different spectral characteristics. For example, relatively thin ice forming within leads exhibits a low albedo and relatively high physical temperature, but the microwave brightness temperature differs dramatically from that of open water. In this example, the problems inherent in comparing lead statistics using imagery of different spatial resolutions and spectral characteristics is apparent: application of thresholds to the three data types yields 1.1% lead-covered area in the Landsat image, 12.8% in the AVHRR (which includes apparent low cloud with substantially warmer temperatures than the ice surface), and 5.4% lead-covered area in the KRMS image. Depending on which image type is used, these lead-fraction estimates would yield roughly an order of magnitude difference in the estimate of turbulent heat transported into the atmosphere from the warmer ocean.

While there are advantages to comparing lead statistics derived from different types of imagery, such a study is complicated by different acquisition times, spectral bands of the various sensors, and geolocation problems. To alleviate these sources of uncertainty, we choose to work with images of a single data type that are successively degraded in resolution by modeling the transfer function between the initial data and the desired resolution and then sub-sampling. A spatial filter that estimates the point spread function of the Landsat sensor is applied following the methodology presented in Justice et al. (1989). At each degradation cycle, Gaussian

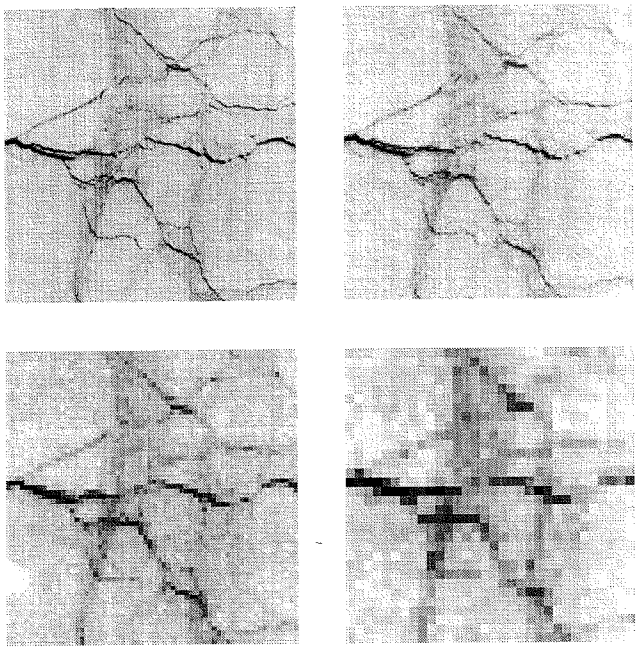

Figure 2. Landsat MSS Band 4 scene of the ice pack north of Alaska in March 1988. Area covered in the images is approximately 80 km^2. The degraded images have pixel sizes of 80 m (upper left), 160 m (upper right), 320 m (lower left), and 640 m (lower right).

random noise is added back into the image to reduce the smoothing effects of the filtering operation.

We start with Landsat MSS Band 4 (0.5–0.6 μm) scenes of the Beaufort Sea, March 1988, with an initial FOV of 80 m (Fig. 2). The fourth-order trend surface is removed from the original grey scale image (Eppler and Full, 1992) in order to correct for brightness variations caused by typically low sun angles in the Arctic. Images with FOVs of 160 m, 320 m, 640 m, and 1280 m are then created using the spatial filter. Each degradation is segmented using a threshold based on the Sobel operator edge detector. This procedure determines the discrete spatial gradient at each pixel in both dimensions. When its histogram is compared with that of the original image, the point of intersection determines an adequate cutoff between a lead and the ice. We note that the lead / not-lead decision is somewhat subjective; linear features from older, refrozen leads, for example, may or may not be included as leads. To differentiate between leads and other low-albedo features such as shadows and isolated open-water areas, valid lead fragments are identified using tests based on width and orientation. Linearity is determined through correlation / regression analysis of pixels within the candidate features. Lead widths are measured perpendicular to the regression line, at 1-km intervals, and the slope of the regression line is the measure of the feature orientation.

In addition to the series of degraded-resolution Landsat images, "synthetic" images are generated as an additional tool to study the effects of spatial resolution on observed lead characteristics. These synthetic images represent lead networks as recorded in a thermal channel; for example, leads and the surrounding ice are assigned different physical temperatures. The reason for using simulated leads is that their geometrical characteristics are completely known. Lead networks are simulated as a Poisson line process, where the mean spacing of lines (leads) is 2500 m and the orientations are random. The lines are assigned thicknesses (widths) following the negative exponential density function:

$$f_w(w) = \frac{1}{\lambda} e^{-w/\lambda},$$

where w is lead width and λ is the mean width. For the simulations, $\lambda = 200$ m based on lead observations derived from submarine sonar data (e.g., Key and Peckham, 1991). For this stage of the study, leads can consist of either open water or thin ice within the surrounding matrix of thick ice. Three ice thicknesses are used: 0 (open water), 5, and 15 cm; the surrounding thick ice has a thickness of 2 m. Corresponding temperatures are 271 K, 256 K, 248 K, and 235 K. In the simulation, ice thicknesses within leads are assigned probabilities consistent with ice thickness distributions reported by Maykut (1982). One realization of the Poisson line process is shown in Figure 3. The initial pixel size is

Figure 3. One realization of a lead network simulated by a Poisson line process with thick lines. Pixels sizes are 137.5 m (upper left), 275 m (upper right), 550 m (lower left), and 1100 m (lower right). Grey-scale values represent brightness temperatures.

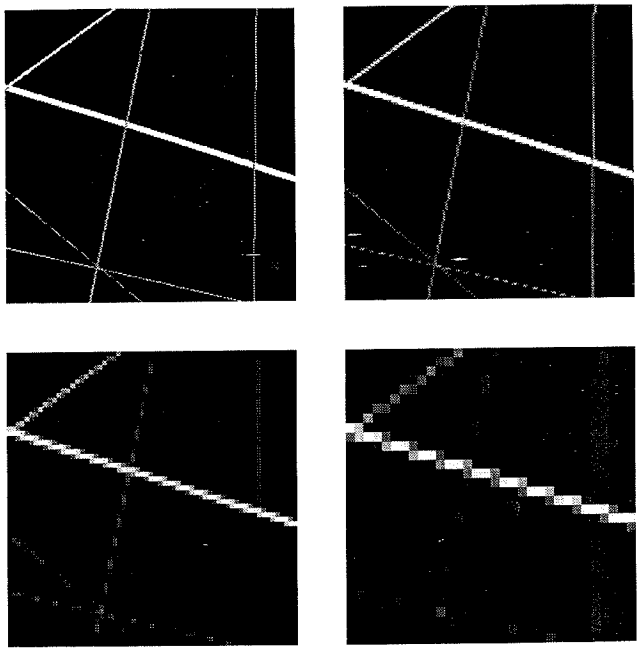

137.5 m, assigned so that the pixel size after the third degradation is 1.1 km, the nominal FOV of the AVHRR sensor at nadir.

OBSERVED CHANGES IN LEAD GEOMETRIES WITH FIELD-OF-VIEW

In this section the geometrical characteristics of leads in the degraded images are described. Results are, of course, specific to the Landsat and simulated images that were analyzed. A discussion of the implications for using lead information extracted from sensors of different field-of-views for heat flux estimates and other applications is deferred until the next section.

The distribution of lead widths corresponding to the images in Figure 2 (degraded-resolution Landsat imagery) is shown in Figure 4. The disappearance of small leads due to reduction in contrast and the apparent increase in the relative frequency of large leads as pixel size increases can readily be seen. In this particular Landsat sample, we find that leads narrower than approximately 250 m disappear as the resolution of the Landsat image is degraded to 320 m and 640 m. However, the criteria for how a given lead will "grow" in width or disappear during image degradation depends on contrast in reflectance of the lead compared to that of the surrounding ice. For example, a narrow, open-water lead might increase in apparent width while decreasing in contrast as pixel size increases during the first degradation. However, in the subsequent degradation, the lead may "disappear" as the average of the subresolution lead and the surrounding ice raises the pixel reflectance above a given threshold. A narrow refrozen lead, in comparison, might disappear during the first degradation since the brightness contrast between the thin ice in the lead (rather than open water in the previous case) and the surrounding ice is initially smaller.

Orientations of leads can also be expected to change if the orientations are anisotropic (i.e., have a preferred orientation). An illustration of this is shown in Figure 5 for the Landsat image in Figure 2. Results from other Landsat scenes show similar patterns and are therefore not shown. Lead widths and orientations from the simulated lead networks (e.g., Fig. 3) exhibit similar dependencies on pixel size, although orientations do not change substantially as with the real data since the basic pattern is isotropic.

Figure 6 shows the change in mean lead width as a function of field-of-view for six Landsat images. We find that while the manner in which widths of individual leads changes is highly variable, the mean lead width, averaged over the entire image, seems to change in a more predictable way. This is a potentially important property since "true" mean lead widths might then be predicted based on measurements from a lower-resolution sensor.

Figure 4. Lead width distributions for the Landsat image series in Figure 2. Widths are grouped in 100-m bins.

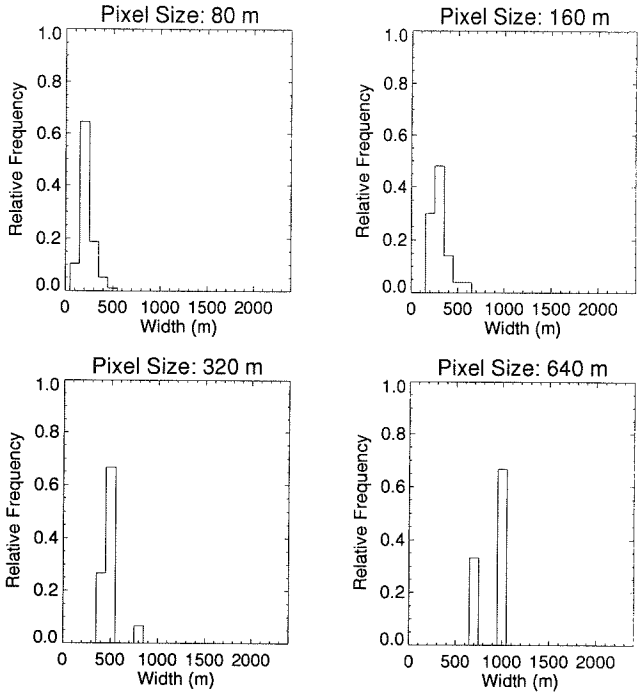

Figure 5. Lead orientations for the degraded Landsat series shown in Figure 2. Orientation is the angle that a lead makes with the horizontal axis, measured counterclockwise.

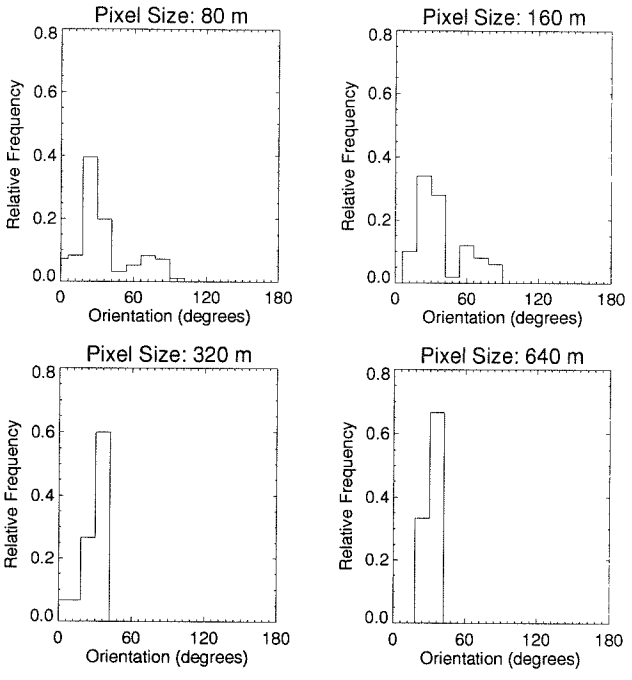

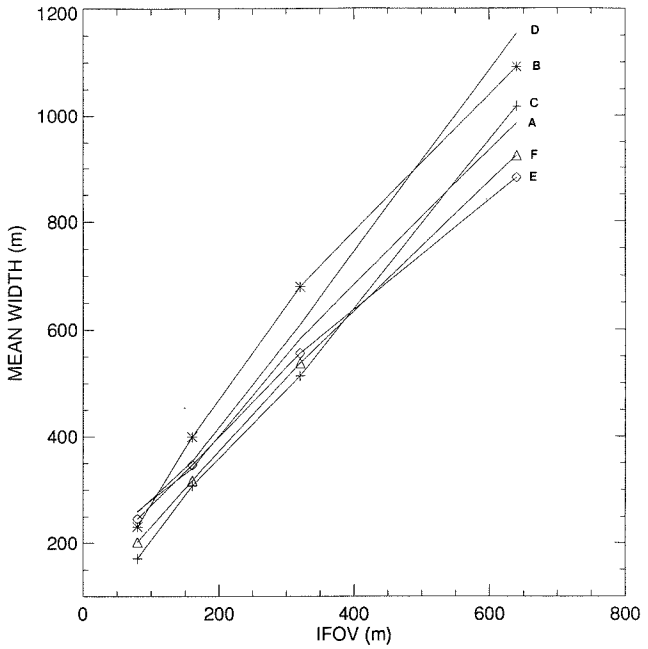

Figure 6. Change in mean lead width as a function of field-of-view for six Landsat images.

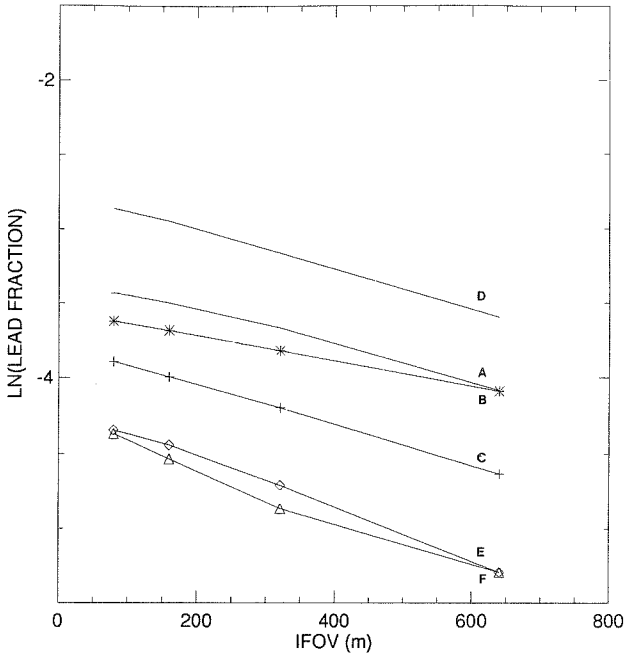

Figure 7. Change in total lead fractional area as a function of field-of-view for six Landsat images.

The change in total lead areal coverage as a function of field-of-view is illustrated in Figure 7 for the six Landsat images. The change in area fraction with increasing pixel size is generally exponential. The actual rate of change is, however, sensitive to the threshold levels used. In fact, it can be shown that lead area fraction may either increase or decrease with increasing pixel size depending on the threshold used. The theoretical reasons for this are discussed in a later section. However, when the same thresholding method is used, the lead fraction difference between degradation cycles varies in a predictable way. In other words, though the definition of a "lead" in the original image is still subjective, once defined it remains consistent throughout the range of degradations.

CONTRAST EFFECTS AND THRESHOLD SELECTION

The reason for the change in lead geometrical characteristics with sensor resolution is now examined in terms of contrast. We define the *normalized contrast* as a ratio based on the target and background temperatures, T_T and T_B:

$$C = \frac{T_T - T_B}{T_B}.$$

Of course, the contrast ratio need not be defined in terms of temperature, so that T_T and T_B could also be reflectance or digital number (DN). Letting p be the fractional area coverage of a lead in a pixel; for example, width / FOV, then the *total contrast*, which takes into account the reduction in temperature contrast as a function of pixel size, is

$$C_{tot} = \frac{[pT_T + (1-p)T_B] - T_B}{T_B} = pC.$$

The change in total contrast can be seen in Figure 2, and is shown in more detail in Figure 8, where four individual leads, each with a different initial contrast, are placed in an image context. The lead at the top of the figure has the lowest initial contrast. The images are degraded as described previously, with noise added initially and at each degradation. The change in the total contrast of each lead from one degradation to the next is shown in Figure 9.

If every pixel in the image is to be labeled as either a lead pixel or not a lead pixel, then some thresholding operation must be used. One possible method is to choose as a threshold the background temperature plus some multiple of its variability σ, say $T_B + 2\sigma$. This threshold can also be expressed as a unitless contrast ratio:

$$\gamma = 2\sigma / T_B.$$

If the total contrast of a pixel is below this value, then the pixel is not a lead pixel. This threshold contrast includes implicitly the effect of the fractional area coverage of a lead within the pixel. It can be used to determine the minimum initial contrast, or *critical contrast*,

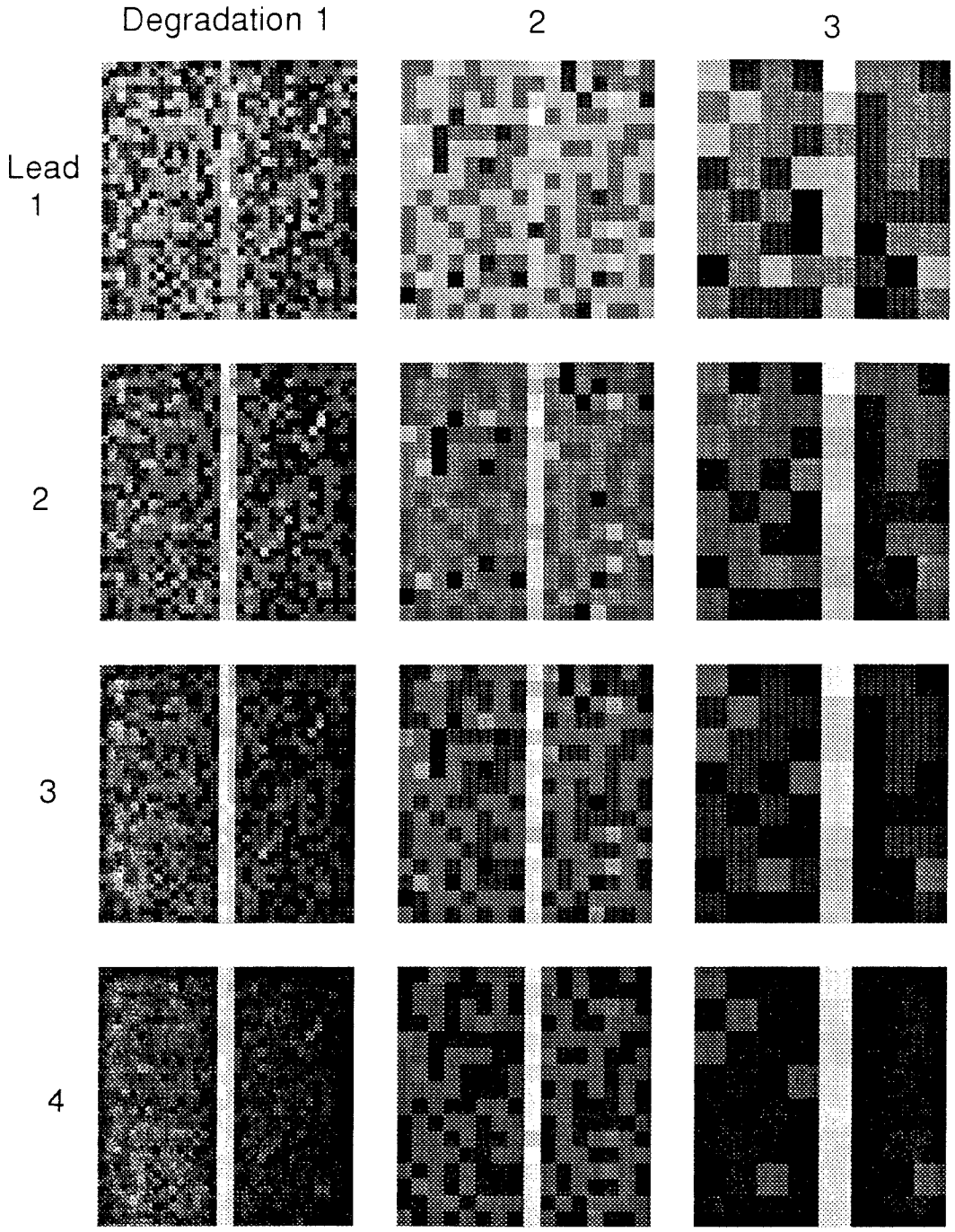

Figure 8. Four single-lead images of varying initial contrast (not shown) degraded three times. Initial lead width is one pixel. Gaussian noise is added after each degradation.

necessary for a lead of a given width in a pixel of a given size to be detectable:

$$C^* = C^*_{\text{tot}}/p,$$

where the asterisk represents a critical (cutoff) value and $C^*_{\text{tot}} = \gamma$.

Figure 10 shows total contrast as a function of the initial contrast and the width / FOV ratio of leads, that is, the combinations of the later two variables that give rise to a specific total contrast. For example, an initial contrast of 0.15 and a p (width / FOV) of 0.15 yields the same total contrast (0.02) as an initial contrast of 0.05 and a p of 0.4. The total contrast can also be considered as the threshold contrast in that any point below a contour chosen as the threshold contrast represents a lead that is not detectable. For example, given a

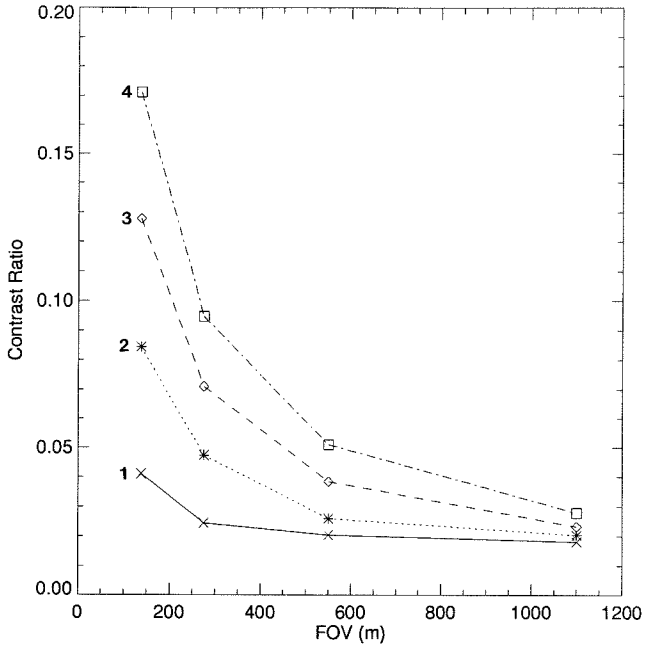

Figure 9. Total contrast as a function of field-of-view for the four leads in Figure 8.

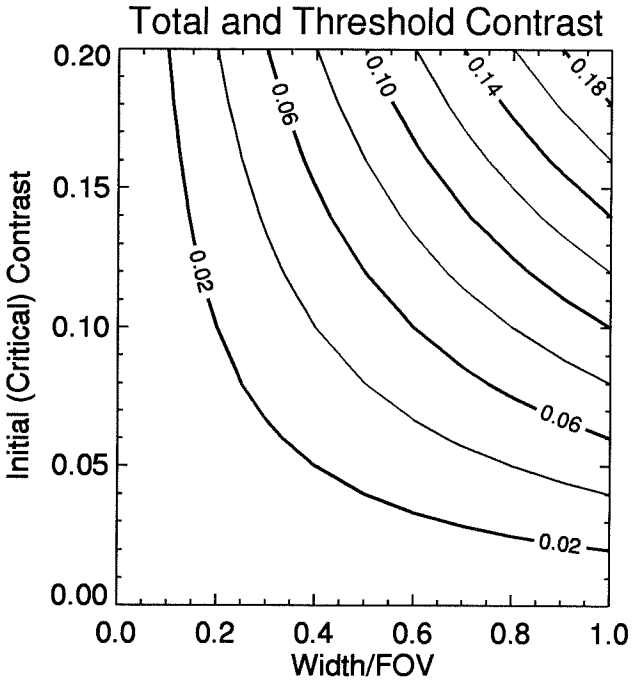

Figure 10. Total contrast as a function of the initial contrast and the width / FOV ratio of leads; that is, the combinations of the later two variables that give rise to a specific total contrast. The total contrast can also be treated as the threshold contrast in that any point below a contour chosen as the threshold contrast represents a lead that is not detectable.

background ice temperature of 240 K with a standard deviation of 5 K, the threshold contrast as defined above is 0.042. If there exists a lead that is 500 m wide passing through a 1 km pixel (so $p = 0.5$), then its initial contrast must be at least 0.084 (which is its critical contrast) for it to be detected. Given a background temperature of 240 K, this critical contrast translates into a lead temperature of 260.2 K.

EFFECTS OF CHANGES IN FIELD-OF-VIEW ON TURBULENT HEAT FLUX

In the previous sections, we showed how sensor field-of-view affects observed lead statistics. In order to better assess the importance of these effects, we placed them in the context of changes in turbulent heat flux from the ocean to the atmosphere.

Changes in both the mean lead width and lead-covered area are considered in the calculation of sensible and latent heat flux as a function of fetch (treated here as the lead width), surface temperature, air temperature, and wind speed using the procedure outlined by Andreas and Murphy (1986). In this approach, a bulk Richardson number defines atmospheric stability that controls convective turbulence based on temperature and wind speed. Convective turbulence combines with the mechanical mixing introduced by the step effect of an air mass in equilibrium with thick sea-ice conditions travelling over the physically rough edge of a lead and the considerably warmer open water or thin ice in the lead. The addition of mechanical turbulence introduced by the ice-lead boundary tends to result in a higher rate of heat transfer from smaller leads compared to larger leads. Thus, for a given areal coverage of leads in an image, a greater number of smaller leads will result in more heat loss to the atmosphere than from a lesser number of larger leads, even though the total amount of open water in the image remains the same. Under the conditions examined by Andreas and Murphy (1986), this decrease in flux as lead width increases becomes negligible for lead widths greater than about 200 m.

To illustrate the effects of changes in lead statistics using different image fields-of-view, we calculate sensible and latent heat flux using the above approach for the data presented in Figure 6 and the associated changes in lead areal coverage in Figure 7. An open-water temperature of $-1.8°C$, wind speed of 5 m s^{-1}, air temperatures of $-28.9°C$ at a reference height of 2 m, ocean salinity of 34 ppt, air pressure of 1000 mb, and a neutral-stability drag coefficient of 1.49×10^{-3} are used to represent typical mid-winter (January) conditions over the Arctic sea ice pack (Maykut, 1978; Andreas and Murphy, 1986). Although leads are often covered by thin ice rather than open water and thus have a lower surface temperature than open water, the assumption that the leads are not refrozen and have a surface temperature of $-1.8°C$ is a useful baseline for our calculations. Turbulent (sensible plus latent) heat flux from leads is calculated using

Table 1. Areally Averaged Turbulent (Sensible + Latent) Flux (W m^{-2}) for Typical January Conditions as a Function of Field-of-View (FOV) for Six MSS Images[a]

	Image					
FOV (m)	*A*	*B*	*C*	*D*	*E*	*F*
80	23.5	19.1	17.4	50.7	10.6	15.0
160	22.2	17.7	14.4	47.0	9.7	12.1
320	19.9	16.1	11.7	41.6	8.2	8.9
640	16.7	14.0	7.9	33.7	5.6	5.3
% Change	29	27	55	34	47	65

[a] The percent change in the flux between FOVs of 80 m and 640 m is also shown.

the mean lead width at each field-of-view and then weighted by the areal coverage of leads for the six MSS images used in Figures 6 and 7 to yield an areally averaged heat flux. Turbulent fluxes from open-water leads under these conditions are around 300 W m^{-2} compared to a flux of nearly 0 W m^{-2} from surounding ice taken to be 3 m thick. Thus, lead fraction and lead width dominate the transfer of turbulent heat through the ice pack during winter. Table 1 shows these areal averages for the six MSS images. Since the effect of increasing the fields-of-view in these examples is to decrease the apparent lead fraction, areally averaged fluxes decrease as field-of-view increases. However, as noted earlier, the choice of thresholds can affect both the magnitude and direction of change in lead statistics with changing FOV. If we assume that the lead widths and lead fractions measured using the 80-m FOV imagery are closest to reality, then the errors introduced by using lead widths and lead fraction measured at a 640 m FOV are substantial—averaging 45% over the six images. Since the change in turbulent heat transfer with changing lead width is greatest for smaller leads, those images with smallest mean lead widths at the 80 m FOV (such as images C and F) are most affected. In the images studied here, where the mean lead width is fairly large, the effect of errors in lead fraction is about five times that of the effect of uncertainty in lead width.

TRANSLATION BETWEEN SCALES

From the previous discussions it is obvious that lead statistics change significantly as a function of field-of-view and that there are important implications of these changes for large-area turbulent heat flux estimates. Is there any possibility of estimating the true lead widths and area fractions from those observed in lower-resolution imagery?

Width Distributions

Given that very small features will generally not be resolved, the issue then becomes one concerning the possibility of using the distribution of lead widths measured at low resolution to estimate the complete or "true" distribution. For example, assume that lead widths x follow a negative exponential distribution with an unknown mean λ. From a sampling point of view, it is useful to treat the distribution of widths as discrete and address the number n_i of leads in bin i that have widths between x_i and $x_i + w$:

$$n_i = \frac{Nw}{\lambda} e^{-x_i/\lambda}, \tag{1}$$

where w is the width of the bin and N is the unknown total number of leads in the spatial area. The idea is that n_i is measured for a few bins and that λ and N are estimated. To accomplish this, (1) is rewritten in linear form as

$$\ln(n_i) = \ln\left(\frac{Nw}{\lambda}\right) - \frac{1}{\lambda} x_i. \tag{2}$$

Letting $a = \ln(Nw/\lambda)$ and $b = \lambda^{-1}$ and solving for a and b by the method of least squares with the observed data, the mean of the distribution and the total number of leads can then be estimated.

Experiments with this model show it to be very sensitive to the bin width and the number of bins, in which leads actually occur in the lower-resolution imagery. This is not unexpected considering that the entire range of x is being estimated in the least squares model by observations in only one part of its range. A more fundamental problem exists with this method: As shown earlier, the widths of the leads observed in the lower-resolution data are probably not the true widths of those leads. Figure 11 illustrates the problem where the actual lead width distribution—which is exponential—in the simulated leads image of Figure 3 is estimated using the above method and the observations from each degraded image. Significant departures from the actual distribution are obvious.

Is it possible to unmix the pixels and thereby obtain the true lead widths? Using a single spectral band, it is not possible when ice of different thicknesses, and thus different reflectances and surface temperatures, is present in the field-of-view. For a brief time during the

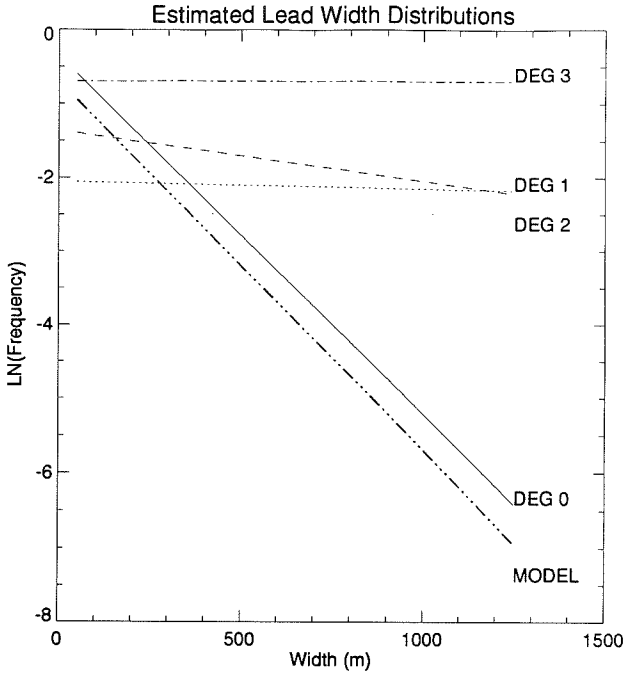

Figure 11. Estimated actual width distributions from observed lead widths at each field-of-view or degradation (DEG0–DEG3) of the simulated lead network shown in Figure 3. Also shown is the model distribution used to generate the leads in the image.

summer when new ice is not forming in the leads, the percentage of open water within the FOV can be calculated with a single spectral band since all leads can be assumed to contain only open water and therefore essentially the same reflectance or temperature. During the winter when no visible-band data are available, no unmixing is possible since leads can consist of a large range of ice thicknesses. During the spring and fall months, the problem can, in theory, be solved using one thermal and one visible-band observation and an energy balance approach as follows. The total contrast of a lead pixel in both a thermal and a visible-band image of the same lead are observed. The mean background (ice) temperature and albedo, T_B and α_B are determined from the data. This leaves two equations with three unknowns:

$$C_{\text{tot},IR} = p\frac{T_T - T_B}{T_B},$$

$$C_{\text{tot},VIS} = p\frac{\alpha_T - \alpha_B}{\alpha_B}.$$

Actually, the target (lead) temperature and albedo are physically related, although the relationship is a complex one. An energy balance model is used to determine the target albedo for a given target temperature (Maykut, 1982):

$$(1-\alpha_T)F_r - I_{\text{ice}} + F_l + \varepsilon\sigma F_T^4 + F_s + F_e + F_c = 0,$$

where α is the albedo, ε is the longwave emissivity, σ is the Stefan–Boltzmann constant, I_{ice} is the amount of shortwave energy that penetrates the ice and does not directly heat the surface, F_r and F_l are the downwelling shortwave and longwave radiation, F_s and F_e are the sensible and latent heat fluxes, and F_c is the conductive heat flux. A flux toward the surface is positive. The energy balance equation is solved for a range of possible target temperatures, $T_B \leqslant T_T \leqslant 273.15$ K, until a combination of p, T_T, and α_T is found that is consistent with the observed total contrasts.

While in theory this method will work, in practice it would be difficult to accurately estimate all the necessary parameters. It is not our purpose here to present methods of retrieving these parameters, but instead we summarize the potential error through an example of the sensitivity of the energy balance approach: If the target albedo α_T can be estimated to within 0.05, for example, the range of p that could satisfy the above equations is 0.455–0.556 for $\alpha_B = 0.7$, a true p of 0.5 and a true α_T of 0.2. With a 1-km FOV this translates into a range in lead widths of 445–556 m, where the true width is 500 m. While the use of physical models can help the unmixing process, we do not expect that we will ever be able to fully resolve the mixture components with existing data.

As can be seen in Figure 6, however, the unmixing of pixels to determine the actual lead widths observed may not be necessary. The fact that the mean lead widths change in a predictable way with increasing pixel size implies that the mean of the width distribution measured at one field-of-view can be used to estimate the mean width at another field-of-view. Even though the rate of change of mean lead width with pixel size depends on the threshold used (not shown), the relationship is approximately linear for a given thresholding operation. This relationship can be utilized as follows. For an image at a given field-of-view, determine the mean lead width. Degrade the image and once again determine the mean lead width using the same thresholding operation as before. The two points define a line analogous to those in Figure 6. The mean lead width at a narrower FOV can then be determined and applied in (2).

Of course, the relationship is not perfectly linear, so that some error in the predicted mean lead width can be expected. As an example, we consider the two images with the smallest and greatest error in turbulent heat flux due to FOV, as given in Table 1, images B and F. The relationships for these two images are among the most nonlinear of those examined. For image B the mean lead width at a pixel size of 320 m is 680 m; degrading that image to a 640 m pixel size would yield a mean lead width of approximately 1080 m, also as indicated. If these two points were then used to extrapolate back to a FOV of 80 m, the estimated lead width

would be 360 m as opposed to the 231 m value actually measured in the imagery. The difference between the turbulent flux calculated for a single lead (no area weighting) whose width is the mean width at 320 m FOV and that calculated at the 80 m FOV is 16 W m^{-2} (4.1% difference) compared to 12 W m^{-2} (3.1%) using the mean width extrapolated to an 80 m FOV from measurements at 320 m FOV. For image F, which showed the greatest sensitivity of turbulent fluxes to field-of-view, the corresponding errors are 25 W m^{-2} (6.3%) and 15 W m^{-2} (3.8%).

Total Area

If lead area fraction in satellite imagery follows a known scaling law, then the "true" area fraction can be estimated from the area fraction determined at any scale. Fractal geometry is type of scaling relationship that has been used in the analysis of geophysical phenomena and deserves mention in the context of lead area. In particular, the stream length-drainage area relationship has been described in terms of fractals (Robert and Roy, 1990). However, in that and related studies the streams have no width and are therefore not applicable to the lead studies presented here. In contrast, Karlinger and Troutman (1992) have examined the "fat" fractal relationship between river channels with finite widths and drainage area. An examination of the data presented in Figure 7 reveals that in general the fractional area coverage of leads decreases exponentially (log-linear) with increasing pixel size, and in some cases the decrease is even linear, so that the log-log relationship described by fractal scaling laws does not appear to apply.

As with lead widths, the rate of change of area fraction with increasing pixel size is not constant, but rather is a function of the threshold used. In fact, the direction of change is also threshold-dependent, so that the lead area may increase or decrease with increasing pixel size. The theoretical reasons for this are examined in Key (1993), where the distributions of the subpixel area fraction of various geophysical fields with known covariance structures are modeled by a Beta probability distribution, and the estimated total area fraction in an image is determined as a function of threshold. Unfortunately, the relationship between digital number (or temperature or reflectance) and the subpixel area fraction can be complex, so that expressing the subpixel area fraction threshold as a DN threshold is often not possible.

Therefore, perhaps the best estimate of the true area fraction of leads in an image is obtained using the procedure outlined earlier for mean lead width: degrading the image once, assuming an exponential or possibly linear relationship, and extrapolating back to a smaller FOV. Of course, the same thresholding operation must be used for both images (the Sobel operator here). As was done in the previous section, the potential error in this method for the Landsat images can be examined using the data in Figure 7. Using image B, lead fraction extrapolated to an 80 m FOV from observations at an FOV of 320 m is 0.031 versus the observed fraction at 80 m of 0.0378. Combining this error with the error in open-water turbulent flux associated with mean lead width as calculated in the previous section, the error in using the extrapolated lead fraction and lead width versus the statistics observed at an 80 m FOV is 5.7% of the areally averaged turbulent heat flux. If the lead statistics are not adjusted for field-of-view, that is, if the lead statistics observed at an FOV of 320 m are used, then the error increases to 15.6%. For image F, the error is 20% using the extrapolated statistics compared to 40.7% percent using the statistics at 320 m. In these two cases, extrapolating the lead statistics reduces the average error in turbulent flux by about 57%.

SUMMARY AND CONCLUSIONS

Given the importance of sea-ice leads for climate processes and the desirability of mapping leads by remote sensing, the accuracy of lead mapping using imagery with different spatial resolutions is a critical issue. To investigate the effect of sensor resolution on lead widths and areal coverage, Landsat MSS data were degraded from 80 m to 640 m fields-of-view, using the modulation transfer function for the sensor. In addition, synthetic images were created where true lead widths and area coverages are known. For the Landsat imagery, the Sobel operator provides an objective and consistent method to segment an image into lead / not-lead areas.

It can be seen that small leads tend to disappear in the coarser resolution data and large leads "grow" primarily by becoming wider. The total lead fraction decreases as field-of-view increases, roughly following a log-linear relationship. Both the rates and direction of change are, however, closely tied to the threshold used in creating the binary image. Lead orientation distributions also change with increasing pixel size, indicating that, in the imagery examined, small leads exhibit different orientations than larger leads. The importance of incorrect lead width distributions and area fraction is illustrated with respect to area-weighted heat fluxes, where the difference between lead statistics derived from images with 80 m and 640 m FOVs translates into an average error in turbulent heat flux of 37%, which includes the combined effects of an apparent decrease in lead-covered area and the increase in mean lead width as FOV increases. If the empirical relationship is applied to extrapolate mean lead width and lead-covered area to correct for scale, the error in the estimate of

areally averaged heat loss is reduced by 57% in the two examples studied.

Although our emphasis was to define the effects of image field-of-view on lead statistics and turbulent energy flux, applications for ice and climate modeling and validation acually require knowledge of the true distribution of leads in the ice pack; that is, the distribution that one would obtain by sampling at a field-of-view small enough to resolve the number and dimensions of all leads. For the applications here, we took the lead information sampled at 80 m to be true. The next step is test how well the observed relationships hold for the interval from 80 m down to 25 m or less. Work is underway to test this using the statistical distributions and extrapolation procedures discussed earlier in combination with imagery at different scales, including ERS-1 synthetic aperture radar data, airborne passive microwave imagery, and aerial photographs.

Of course, the problem is not limited to the scaling effects of leads. Clouds may have an even greater influence on local and regional climate, and the effect of sensor resolution on estimated cloud amount is significant (Key, 1993). Therefore, radiative fluxes computed using satellite-retrieved cloud properties will almost certainly be in error, the magnitude of which will depend on the cloud form, size, vertical placement, microphysical properties, atmospheric conditions, and surface characteristics.

This work was supported by ONR Grant N00014-90-J-1840 and NASA Grants NAGW-2598 and NAGW-2158. Thanks are due to R. Lindsay, D. Rothrock, F. Fetterer, and D. Eppler for useful discussions on the remote sensing of leads, and to A. Schweiger for coregistering the data in Figure 1.

REFERENCES

Andreas, E. L., and Murphy, B. (1986), Bulk transfer coefficients for heat and momentum over leads and polynyas, *J. Phys. Oceanography* 16(11):1875–1883.

Eppler, D. T., and Full, W. E. (1992), Polynomial trend surface analysis applied to AVHRR images to improve definition of Arctic leads, *Remote Sens. Environ.* 40:197–218.

Justice, C. O., Markham, B. L., Townshend, J. R. G., and Kennard, R. L. (1989), Spatial degradation of satellite data, *Int. J. Remote Sens.* 10(9):1539–1561.

Karlinger, M. R., and Troutman, B. M. (1992), Fat fractal scaling of drainage networks from a random spatial network model, *Water Resources Res.* 28(7):1975–1982.

Key, J. (1994), The area coverage of geophysical fields as a function of sensor field-of-view, *Remote Sensing Environ.* 48:339–346.

Key, J., and Peckham, S. (1991), Probable errors in width distributions of sea ice leads measured along a transect, *J. Geophys. Res.* 96(C10):18,417–18,423.

Ledley, T. S. (1988), A coupled energy balance climate-sea ice model: impact of sea ice and leads on climate, *J. Geophys. Res.* 93:15,915–15,932.

LeDrew, E. F., Johnson, D., and Maslanik, J. A. (1991), An examination of atmospheric mechanisms that may be responsible for the annual reversal of the Beaufort Sea ice field, *Int. J. Climatology* 11:841–859.

Maslanik, J. A., and Barry, R. G. (1989), Short-term interactions between atmospheric synoptic conditions and sea ice behavior in the Canada Basin, *Ann. Glaciol.* 12:113–117.

Maykut, G. A. (1978), Energy exchange over young sea ice in the Central Arctic, *J. Geophys. Res.* 83(C7):3646–3658.

Maykut, G. A. (1982), Large-scale heat exchange and ice production in the central Arctic, *J. Geophys Res.* 87(C10): 7971–7984.

Maykut, G. A., and Perovich, D. K. (1987), The role of shortwave radiation in the summer decay of a sea ice cover, *J. Geophys. Res.* 92(C7):7032–7044.

Robert, A., and Roy, A. G. (1990), On the fractal interpretation of the mainstream length-drainage area relationship, *Water Resources Res.* 26(5):839–842.

Shenk, W. E., and Salomonson, V. V. (1972), A simulation study exploring the effects of sensor spatial resolution on estimates of cloud cover from satellites, *J. Appl. Meteorol.* 11:214–220.

Simmonds, I., and Budd, W. F. (1990), A simple parameterization of ice leads in a general circulation model and the sensitivity of climate to change in Antarctic ice concentration. *Ann. Glaciol.* 14:266–269.

Stone, R., and Key, J. (1993), The detectability of winter sea ice leads in thermal satellite data under varying atmospheric conditions. *J. Geophys. Res.* 98(C7):12469–12482.

Townshend, J. R. G., and Justice, C. O. (1988), Selecting the spatial resolution of satellite sensors required for global monitoring of land transformations, *Int. J. Remote Sens.* 9(2):187–236.

Wielicki, B. A., and Welch, R. M. (1986), Cumulus cloud properties derived using Landsat satellite data, *J. Clim. Appl. Meteorol.* 26:261–276.

Woodcock, C. E., and Strahler, A. H. (1987), The factor of scale in remote sensing, *Remote Sens. Environ.* 21:311–316.